Robotica (2016) volume 34, pp. 2309–2329. © Cambridge University Press 2015
doi:10.1017/S0263574714002938

A multi-configuration kinematic model for active drive/steer four-wheel robot structures

Edgar A. Martínez-García*, Erik Lerín-García and Rafael Torres-Córdoba

Institute of Engineering and Technology, Universidad Autónoma de Ciudad Juárez, Juárez, Chihuahua, México

(Accepted December 18, 2014. First published online: January 30, 2015)

SUMMARY

In this study, a general kinematic control law for automatic multi-configuration of four-wheel active drive/steer robots is proposed. This work presents models of four-wheel drive and steer (4WD4S) robotic systems with all-wheel active drive and steer simultaneously. This kinematic model comprises 12 degrees of freedom (DOFs) in a special design of a mechanical structure for each wheel. The control variables are wheel yaw, wheel roll, and suspension pitch by active/passive damper systems. The pitch angle implies that a wheel's contact point translates its position over time collinear with the robot's lateral sides. The formulation proposed involves the inference of the virtual z-turn axis (robot's body rotation axis) to be used in the control of the robot's posture by at least two acceleration measurements local to the robot's body. The z-turn axis is deduced through a set of linear equations in which the number of equations is equal to the number of acceleration measurements. This research provides two main models for stability conditions. Finally, the results are sustained by different numerical simulations that validate the system with different locomotion configurations.

KEYWORDS: Kinematics; Control law; Four wheel; Active steer; z-turn axis; Accelerometer.

1. Introduction

Wheeled mobile robots (WMRs) are rolling devices capable of performing locomotive tasks on surfaces solely through the actuation of wheels in contact with the surfaces of displacement. In the simplest case, the wheel is connected to the robot's body using the horizontal wheel axis (conventional and/or Swedish wheel) or using the vertical wheel axis (centred and off-centred wheels). In the most complex cases,[4,5,8] the wheel is connected to the robot's body through a mechanical link assembly, as we are proposing in the present study. The link assembly allows relative motion between the mechanical frame and the surface on with which, there exists an area of rolling contact.[1] Some link assemblies contain passive suspensions,[12,24] and while others including this particular study contain active suspensions.[5,8,11,15,31,37] In addition, there are two steering methods to change the displacement direction of WMRs: skid steer and explicit steering. For the models in this manuscript, none of the wheels involved are passive; all are combined as active driven or active steerable.

The WMRs are modeled as mechanical bodies supported by wheel assemblies, which enable the kinematic connections with the robot's body, steering functions, and the driving controls of the wheels. It is well known that rolling without sliding or slippage *can* only be guaranteed under certain particular conditions. There are two circumstances in which wheel sliding or slippage may occur: when the pure rolling of the wheel is not compatible with the steering and driving controls, and when the inertial forces in the robot structure exceed the friction force between the wheel and the travel surface.[1,24] The placement of the wheels on the robotic structure and the wheel restrictions contribute to the robot's mobility. There traditionally exist four types of wheels: conventional, centred,

* Corresponding author. E-mail: edmartin@uacj.mx

off-centred, and Swedish. The centred wheel is the most widely used type of wheel (i.e., wheelchairs, automobiles, motorcycles), and the possession of two DOFs allows for travel over a surface in the direction of the wheels' orientation and rotation about the point-of-contact on the traveling surface.[1]

The WMR's degree of holonomy is determined by the value of mobility and manoeuvrability (how quickly the traveled direction can be changed). This value is measured by the wheels' restriction, and WMRs are classified as systems with holonomic and non-holonomic properties according to their degrees of mobility m and steerability s.[6]

Holonomic WMRs are able to move in all DOFs available in the workspace; thus, this kind of robot does not have mechanical constraints that limit mobility. Accordingly, the non-holonomic robots are not able to move in all directions because they have kinematic constraints in their locomotion structure (one example of this mechanical structure is the "*like-car*" robots). A WMR does not typically include suspension devices, and the robot displacement is obtained by quantization of the wheels' rolling; hence, the slippage (scrubbing) or skidding effects are not usually considered when regarding indoor structured navigation surfaces. Measurements of distance and direction displacement are obtained by odometry techniques. Wheel skidding and slippage are present when navigating in outdoor, unstructured, uneven surfaces, and in dynamic environments.[15,27] In some all-terrain robots, suspension systems are included, primarily in order to maintain contact between the wheel and the ground for as long as possible and to reduce frame movements generated by rolling over uneven surfaces. WMRs with active suspension systems are capable of modifying the friction forces between the wheel and the contact point via surface displacement, as well as changing their centre of mass to avoid overturns while moving through irregular and sloping terrain by modifying and adjusting their suspension linkages and joints.[4,11,14,15,17,18,24,31,35,37] In all-terrain WMRs, the use of odometry to obtain distance and direction displacement is usually not enough; to improve distance and direction estimations, the addition of proprioceptive devices such as inertial measurement units, GPS, and optical speed sensors[4,7,35] is needed. Since all-terrain surfaces are defined by a Cartesian axis (x,y,z), a possible solution for navigating such surfaces and avoiding obstacles is to use holonomic or kinematic redundant vehicles.[3,22]

The present manuscript is organized as follows. Section 2 provides an analysis of various issues found in recent related works. Section 3 discusses the stated problem of 4W kinematic structures and offers some considerations. In Section 4, we provide an analysis of our mechanical design suspension and discuss its kinematic restrictions. Section 5 includes a description of the z-turn axis and its importance to and impact on the robot's kinematics. Section 7 presents the kinematic control law that governs an arbitrary robot's locomotion configuration. In Section 8, a set of multiple locomotion configurations are illustrated and provide evidence of the proposed kinematic model through numerical simulations. Finally, Section 9 offers some concluding comments.

2. Related Work

The evolution of WMR research on kinematics modeling shows growth from simple mobile robots moving on flat terrain,[1,6,14,28] to high-mobility rovers designed for uneven surfaces.[8,17,31] A skid-steer WMR named Scarab was developed for lunar missions in polar craters.[4] The kinematics for Scarab turned out to be very similar to the Jet Propulsion Laboratory's "Sample Return Rover" (SRR).[14] The Scarab rover comprises four wheels directly and independently driven and passive kinematic suspension with active posture adjustability. This posture adjustability allows the rover to drive cross-slope and turn switchbacks to better ascend and descend unconsolidated soil. The robot uses an on-board inertial measurement device and optical ground speed sensor to estimate position and velocity and employs laser range scanners to build models of the surrounding terrain to detect obstacles and determine safe and efficient paths. In our previous work,[24] a less evolved skid-steer WMR with a spring-mass suspension was described.

Since odometry-based trajectory control is not efficient on uneven surfaces and in skid-steer vehicles, this research uses a home-made inertial module arrangement to measure the acceleration along and across the vehicle body. The information obtained is used to infer the non-visible z-turning axis, which is limited by the imaginary rectangle created by the contact points of the wheels. The kinematic model of this WMR includes the kinematic restrictions of centred wheels, and the trajectory control is modelled by the ICR and the z-turning axis.

Cordes *et al.*[8] introduces locomotion modes for a planetary rover comprised of four-wheeled legs with an active suspension. Each wheel leg provides a total of six DOFs. This type of suspension allows a wide range of postures and drive modes for the rover. In the article, motion due to the commanded velocities of the platform is calculated based on wheel constraints; wheel slippage or skidding are not considered. Reina[27] describes a proposal for a four-wheel drive/four-wheel steering (4WD4S) robot; the cross-coupled controller described *therin* reduces synchronization errors to eliminate wheel slippage. The displacement of the rover is by the explicit rolling of wheels and the orientation of the orthogonal plane of wheels to the same ICR. 4WD4S is a relatively new technology in use that improves manoeuvrability of robotised vehicles. Research on 4WD4S has been conducted,[8,14,23,27,36] but there is a limited amount of research related to the problem of the trajectory control of four-wheeled robotic structures comprising of independent drives and independent steering.[24] 4WD4S vehicles are examples of redundant WMRs. 4WD4S technology has been used in farm vehicles such as tractors since 1910, and in a four-wheel steer off-road car in 1913 manufactured by the Caldwell-Vale company.[19] In the automotive field, the 4WD4S system has been used by Mercedes Benz, Honda,[13] Mazda,[33] Nissan,[34] and Jeep, which in 2005 launched the all-terrain vehicle called "Hurricane".[32] The contribution and novelty of the present research work is the presentation of a direct/inverse kinematic control law for an all-active drive-steer 12 DOF robot-type. Some approaches present a control law only for especial active configurations.[9,21,30,38] This control law allows a kinematic multi-configuration control that ranges from nearly to fully holonomic modes. In this approach, the wheels' positions are mobile and collinear at the lateral sides. Thus, in combination with the robot body's arbitrary acceleration measures, wheels positions are deployed to infer the robot body's vertical spin axis (z-turn). The robot's z-turn axis is used as a pivot to determine the instantaneous angular moment in order to state equilibrium conditions. One novelty of our research is the robot's kinematic structure design, which is a special mechanical case of 4WD4S systems. We present a suspension mechanical system featuring three DOFs per wheel. We define the wheel's yaw β, the wheel's roll angle φ, and an uncommon characteristic regarding mobility based on the wheel contact point location controlled by the suspension angle γ. Other works have presented vertical motion suspension,[10] but the authors of the present manuscript are not conscious of other works dealing with collinear mobile wheel position correlated to inter the z-turn axis. Our contribution considers z-turn axis mobility within a trapezoid-like *xy*-plane, as scoped by the instantaneous wheels contact point. Our work presents a set of linear equations in terms of accelerations measured at arbitrary locations on the robot's body to infer the robot's z-turn position. Each acceleration measurement represents a linear equation, and at least two measurements are enough to infer the z-turn axis coordinates. Standard approaches deploy the robot's centre of gravity as the main centre of rotation.[10,30,38] Our general control law is based on purely kinematic differential equations. Our contribution seeks to determine how to control the 12 DOF geometry of motion from both inverse and direct solutions. We consider that in disclosing precise kinematic models, the geometry of motion will provide numerous future advantages. In addition, it will facilitate future dynamic analysis, because dynamic models have their origins in higher-order derivatives of kinematic differential equations. Since our mechanical design is original, the first step is to present an exhaustive kinematic analysis. In addition, most studies treat a large number of dynamic problems of wheeled vehicles by assuming forces (i.e., using Newton's second law) and, approaching skid-steer inferences on trajectory tracking control,[2,10,20,30] assuming an *a priori* knowledge of the kinematics.[9] The proposed method to infer the spinning of a robot's body with respect to its own vertical rotation axis differs from approaches where the centre of mass or the ICR are inferred along the robots longitudinal axis.[2,21] In addition, some approaches are based on the Lyapunov stability criteria.[30] Our contribution presents a formulation stating two stability conditions of the angular moment and the tangential force of the wheels' contact point with respect to the z-turn instantaneous location.

3. 4W Kinematic Structures

This study covers analyses concerning the kinematics of all-active drive-steer four-wheel systems. Usually, full-active systems require more mathematically complex models compared to combined passive-active systems. This is because full-active systems explicitly require a function that models each control variable. In addition, some geometric advantages are met when using active features:

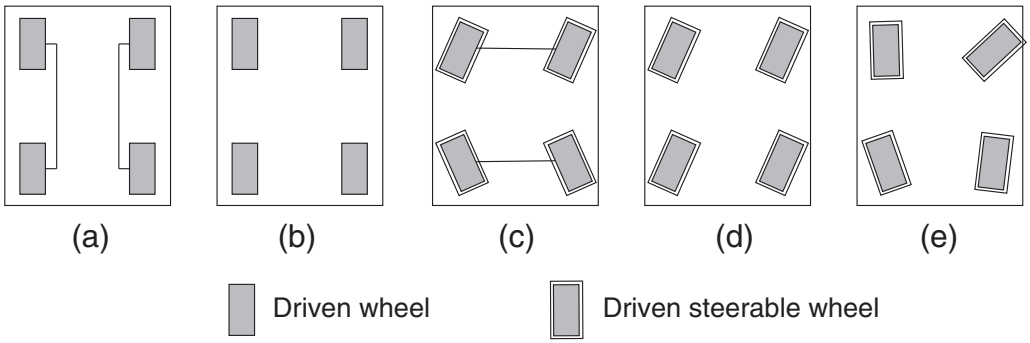

Fig. 1. 4W robot locomotion modes. (a) Lateral differential drive; (b) asynchronous fix-driven wheels; (c) longitudinal differential drive/steer; (d) all-wheel synchronous drive/steer; (e) all-wheel asynchronous drive/steer.

1. With combined passive drive and active steering, the degree of controllability is poorer than full-active driving because wheels lose the ability to move forward/backward at individual contact point speeds.
2. With combined passive steering and active driving, the system loses holonomic properties, and increases the number of geometric constraints. With active-steer systems, the holonomic capabilities allow movement to any Cartesian location at any time.
3. With all-active drive/steer DOFs, wheeled systems behave fully holonomic manner. Nevertheless, special configurations could be set (Table I) to behave in a nearly holonomic manner.
4. Since all-active systems have more DOFs, they can claim greater controllability over manoeuvrability and stability. Passive systems impose more geometrical restrictions, which reduce the number of DOFs.
5. Full-active systems have advantages over combined partial-passive systems when feasibility and reliability in manoeuvrability are demanded to navigate complex terrain surfaces.
6. Although our proposed kinematic control-law model is an aggregation of different combined active/passive systems, its kinematic steer-drive features could be modified to behave as passive features by free-servoing modes for very particular interests.
7. Because all-active drive-steer systems allow multiple kinematic configurations, they provide diverse advantages for self-adaptation to different topographic surface features.

In all-active 4WD4S systems, there are a number of possible locomotive configurations that the kinematics may yield. Some locomotive configurations are illustrated in Fig. 1, and described below.

1. Lateral differential drives with no steering wheels: the robot's orientation is given through lateral control using left/right differential wheel speed to change the robot's angular velocity.[16]
2. Independent or asynchronous 4W-driven without active steering: the robot's orientation is controlled by wheels with differential speeds that contribute to angular velocity.[24]
3. Longitudinal differential drive/steer: the rear wheels are synchronous in steer/drive tasks. The front wheels are synchronous in drive/steer as well.
4. Synchronous driving/steering system, commonly known as crab steering: in this locomotion mode all the wheels have the same turning angle, and the orientation of the vehicle in the global plane is not affected by the wheels' turn angle.[26]
5. Front and rear asynchronous driving and steering: the orientation of the vehicle in the global plane depends on the velocities and steering angle contributions of the wheels.

Figure 1 matches the 4W categories described in Table I. It shows the different configuration modes of 4W systems and shows how driven wheels and steer wheels are configured. In terms of holonomy, we consider robotic structures of 4W contact regions in this manuscript. According to the categories laid out in Table I, we have different locomotive configuration modalities with respect to wheel rolling speeds $\dot{\varphi}$, and steer β.

This manuscript introduces a mechanical design of a WMR, in the category of a 4WD4S displayed in Fig. 2. The kinematic design possesses 12 DOFs with 3 DOFs per wheel, including a spring-mass-damper angle (γ), a wheel-rolling angle (φ), and a wheel-steering angle (β). Depending on

Table I. 4WD4S main configuration modalities (NH: Non-holonomic, H: Holonomic).

4WD configuration modes					
	Holonomy	Speeds	Description	Steer	Figure 1
1	NH	$\dot{\varphi}_r, \dot{\varphi}_l$	2 differential drives.	–	(a)
2	NH	$\dot{\varphi}_1, \ldots, \dot{\varphi}_4$	4 differential drives.	–	(b)
3	H	$\dot{\varphi}_f, \dot{\varphi}_r$	Rear wheels, front-wheels drive/steer.	β_f, β_r	(c)
4	H	$\dot{\varphi}$	1 speed, 1 steer.	β	(d)
5	H	$\dot{\varphi}_1, \ldots, \dot{\varphi}_4$	4 drives, 4 steers.	$\beta_1, \ldots, \beta_4$	(e)

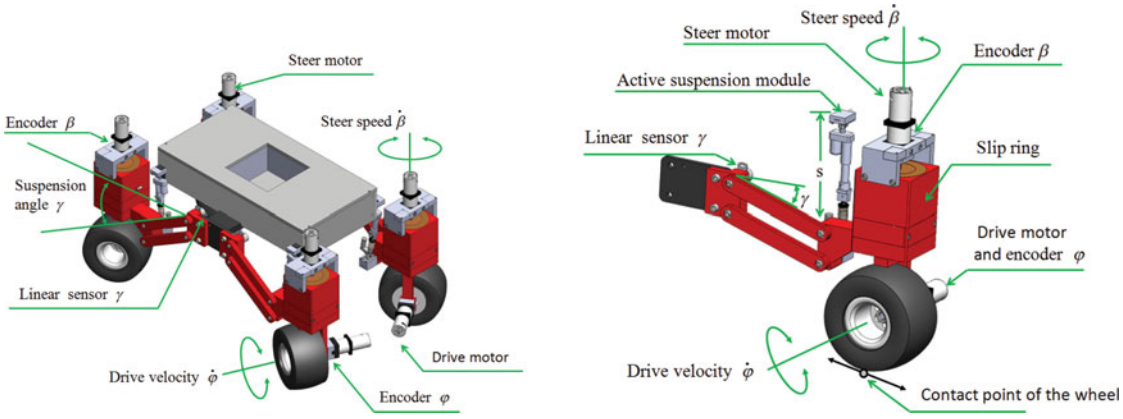

Fig. 2. Design of the 4W robot mechanical prototype (above) and one-wheel suspension assembly (below).

the locomotion configuration mode adopted, when the number of this variables in use is greater than three (x, y, θ), the resulting mathematical system is considered with kinematic redundancy. An advantage of this complex structure, is that its capability to support a large number of DOFs allows different holonomic configuration modes to be featured. Such a structure automatically allows for the setup of multiple locomotive configurations for a diversity of robotic application tasks. For such reasons, a suitable kinematic set of control laws must enable the robot's controllability and manoeuvrability accordingly. Figure 2 depicts several suspension elements proposed for the wheel-suspension assembly:

1. Two DC motors with encoders, one for the steer (β), another to drive (φ).
2. One slip ring to transmit electrical signals between the robot, the motors, and the encoders.
3. Articulated arms with a sensor angle measurement (γ).
4. Active suspension modules with pressure sensors and linear actuators, however these variables are not treated within the scope of this manuscript.

The lateral mobility restrictions of the robot's wheels (orthogonal forces) are also called the nonslip kinematic condition. Figure 3 depicts a top view of the 4W structure kinematics. The wheels' instantaneous angular velocities are denoted by $\dot{\varphi}_1, \ldots, \dot{\varphi}_4$.

Likewise, the wheels' steering angles are defined by $\beta_1, \ldots, \beta_4$, which represent their values within the robot's attached coordinate frame. The locations of the wheels' contact points are given in polar form by $\alpha_1, \ldots, \alpha_4$, with their respective distances l_i, $\forall\, i = \{1, \ldots, 4\}$ with respect to the robot's geometric centre.

Thus, the orthogonal kinematic component restrictions for fixed and centred wheels is described by,

$$\begin{bmatrix} \cos(\alpha+\beta) & \sin(\alpha+\beta) & l\sin\beta \end{bmatrix} \mathbf{R}(\theta)\dot{\boldsymbol{\xi}} = 0, \tag{1}$$

where $\dot{\boldsymbol{\xi}}$ is the robot's posture and $\mathbf{R}(\theta)$ is the Euler rotation matrix. This is the kinematic constraint for each of the four wheels, which produce the robot's entire motion behaviour. We started our reasoning

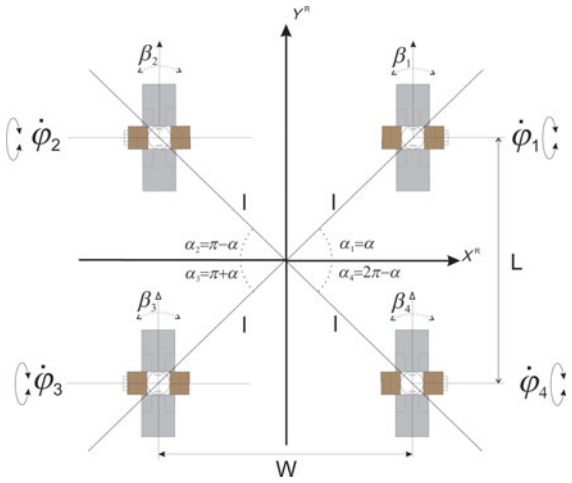

Fig. 3. Top view of a 4W drive-steer robot's kinematic configuration.

following the reported method of nonslip kinematic conditions, and the notation established.[6,29] Thus, *working* from Eq. (1), the matrix of kinematic constraints is defined by $\mathbf{K}_1$

$$\mathbf{K}_1 = \begin{pmatrix} \cos(\alpha+\beta_1) & \sin(\alpha+\beta_1) & l\sin(\beta_1) \\ -\cos(\alpha-\beta_2) & \sin(\alpha-\beta_2) & l\sin(\beta_2) \\ -\cos(\alpha+\beta_3) & -\sin(\alpha+\beta_3) & l\sin(\beta_3) \\ \cos(\alpha-\beta_4) & -\sin(\alpha-\beta_4) & l\sin(\beta_4) \end{pmatrix}. \tag{2}$$

The fixed-wheels matrix $\mathbf{K}_1$ is obtained from the orthogonal kinematic restrictions of all the involved fixed conventional wheels in a 4WD4S structure. In addition, the kinematic conditions for the centred steerable wheels are given in matrix $\mathbf{K}_2$. The resulting mobility capability using the nonslip conditions yields a mobility degree of $\delta_m = 0$ and a steering degree of $\delta_s = 3$

$$\delta_m = 3 - rank\{\mathbf{K}_1\}$$

and

$$\delta_s = rank\{\mathbf{K}_2\}.$$

The numeric value 3 arises from the number of DOFs in the robot's plane of mobility: *x, y,* and θ. In our particular case (i.e., 4WD4S structure), this factor uniquely includes centred, steerable wheels. Thus, both matrixes are $\mathbf{K}_1 = \mathbf{K}_2$. This is because the rank$(\mathbf{K}_1) = 3$. Moreover, hereafter $\mathbf{u}(t)$ is the control input vector, so the general formulation for the posture kinematic model is $\dot{\mathbf{z}} = \mathbf{B}(\mathbf{z})\mathbf{u}(t)$, obtained from the product of transposing the orthogonal rotation matrix $\mathbf{R}(\theta)^T$ and the vector solutions (the null space vectors) of $\mathbf{K}_2$, described by $\Sigma(\mathbf{K}_2)$ as

$$\dot{\mathbf{z}} = \mathbf{R}(\theta)^T \Sigma(\mathbf{K}_2)\mathbf{u}. \tag{3}$$

Since the rank$(\mathbf{K}_2)$ is equal to 3, it is not possible to obtain the posture kinematic model because the null space vector for $\mathbf{K}_2$ has a dimension of zero.

$$\Sigma(\mathbf{K}_2) = \mathbf{0}. \tag{4}$$

Therefore, a real mathematical solution for this algebraic problem is tackled from a different kinematic approach in the next sections.

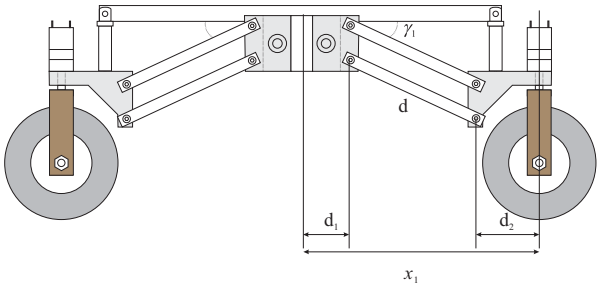

Fig. 4. Robot suspension system (side view).

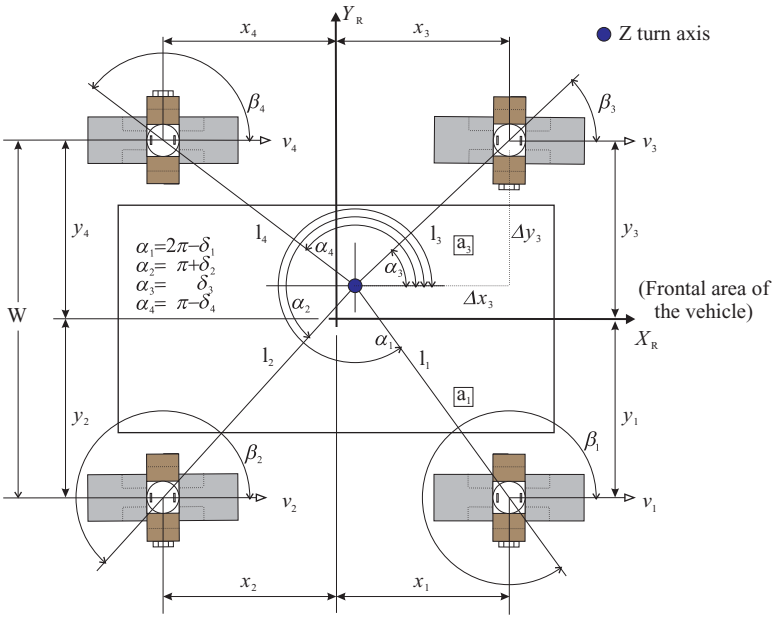

Fig. 5. 4WD4S: Kinematic analysis.

4. Damper Kinematic Constraints

This section presents an analytical discussion of wheel posture kinematics. We model pure rolling conditions affected by the suspension's damper effects. Figure 4 depicts the suspension's mechanical parameters. x_{w_i} is the wheel position along the robot's longitudinal axis and this value refers to the wheels' contact regions, defined by Eq. (5). x_{w_i} varies as the suspension's angle γ_i changes over time. Such wheel variation in translation affects the robot's global controllability and manoeuvrability. This manuscript states in a general form that the wheels' locations changes over time. A wheel's coordinates along the robot's fixed longitudinal axis are x_i, as depicted by Fig. 5. Coordinate values along the robot's transversal axis are y_i, and they are constant for each wheel, as denoted by Eq. (6).

Definition 4.1. Let us define the general robot's wheel position as $(x_{w_i}, y_{w_i}) \forall\, i = \{1, \ldots, 4\}$.

$$x_{w_i} = d_1 + d_2 + d\cos(\gamma_i) \tag{5}$$

with d, d_1, d_2 as depicted in Fig. 4. Likewise,

$$y_{w_i} = \begin{cases} -\frac{W}{2}, & \pi < \alpha_i < 2\pi \\ \frac{W}{2}, & 0 < \alpha_i < \pi. \end{cases} \tag{6}$$

In addition, the model for γ_i is given by the active suspension system. Let us define the following parameters: Δ_s is the suspension offset that sets the device's fixed height (given in m); m is the

spring mass (in kg); κ_r and κ_v are the restitution and viscous coefficients, respectively; g is the gravity acceleration constant (m/s^2); and finally, $\dot{y}_s$ and $\ddot{y}_s$ are the instantaneous velocity (m/s) and acceleration (m/s^2) of the spring-mass elongation, respectively.

Proposition 4.1. *Wheel contact points prevail with no change when steer angles are* $|\beta_i| \geq \frac{\pi}{4}$, *and no damper effects exist.* $\kappa_r = 1$, *and* $\kappa_v = 0$. *The gravitational force exerts no affects over the wheel contact points.*

$$\gamma_i = \arcsin\left(\frac{\Delta s}{d}\right) \tag{7}$$

Corollary 1. *With no damper effects, it is assumed that the z-turn axis is placed on the robot's geometric centre. Hence, this location is taken as a common reference through* l_i.

$$l_i \sin(\alpha_i) = x_{w_i}. \tag{8}$$

Three linear equations that project x^{w_i} *follow. Since the model is already known from a wheel plane perspective, then the expression* (5) *is substituted. A first equation approach is proposed:*

$$l_i \sin(\alpha_i) - d_1 - d_2 - d\cos(\gamma_t^i) = 0. \tag{9}$$

A second equation approach is defined:

$$y_{w_i} \tan(\alpha_i) - d_1 - d_2 - d\cos(\gamma_i) = 0. \tag{10}$$

And a third mathematical approach is offered:

$$\frac{y_{w_i}}{\cos(\alpha_i)} - d_1 - d_2 - d\cos(\gamma_i) = 0. \tag{11}$$

The robot's global motion behaviour is given critically by the instantaneous value of γ_i. An electric adjustable resistance (potentiometer) is used as a linear measurement device to obtain direct measurements $\hat{\gamma}_i$. Nevertheless, a set of functional forms for γ_i are proposed, in accordance with the actual terrain and manoeuvrability of the situation.

Thus, two more propositions for γ_i behaviour are stated that are suited to different situations. The following propositions assume magnitudes of l_i as variables and converge to the z-turn location (x_z, y_z).

Proposition 4.2. *Damper effects are restricted to* $v_t = v_{t-1}$, $\forall t$, *steer angles* $\beta_i = 0$, $\forall i$, *and* (x_z, y_z) *is located at the robot's centroid as a consequence of* $\ddot{y} = 0$.

$$\gamma_i(\dot{y}) = \left(\frac{mg - \kappa_v \dot{y}_s + \Delta s}{\kappa_r d}\right). \tag{12}$$

Proposition 4.3. *Damper effects have no restrictions, and* $v_t \neq v_{t-1}\,\forall t$, $a_t \neq 0$, $\beta_i \neq 0$, *and* (x_z, y_z) *varies its location.*

$$\gamma_i(\ddot{y}_s, \dot{y}_s) = \arcsin\left(\frac{mg - m\ddot{y}_s - \kappa_v \dot{y}_s + \Delta_s}{\kappa_r d}\right). \tag{13}$$

5. Instantaneous Z-Turn Axis Model

In this section, a mathematical model is proposed to infer the z-turn axis location. The z-turn is a virtual axis that implicitly governs the robot's body yaw speed w.r.t. its rotation point. There is not any existing sensor device to measure (x_z, y_z). However, we introduce an approach to infer this on-line by

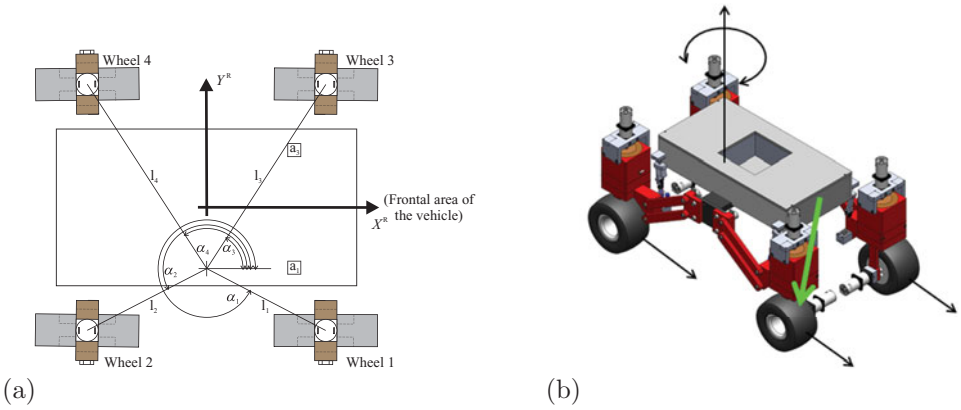

Fig. 6. (a) The z-axis location is displaced from the robot's centroid; (b) the robot's direction (green arrow) is affected by the z-turn and wheels' behaviour.

deploying two-axis accelerometer devices on board (Fig. 6). This is a contribution approach where the z-axis location is used to control the robot's manoeuvrability, forcing it to reach a desired posture regardless of slip/skid effects.

We state in this manuscript that the z-turn region of translation is scoped by the wheels' location (x_{w_i}, y_{w_i}). Inertial accelerometer devices at fixed locations are deployed to infer (x_z, y_z) by means of their instantaneous acceleration measurements over time. Velocities in local inertial systems are deduced by numerical integration w.r.t. time.

Let us define a velocity vector $\boldsymbol{v} = (\dot{x}, \dot{y})^\top$ for each robot's inertial device on board. In accordance with Fig. 5, let us represent the two accelerometer devices a_1 and a_3 as they match the wheel number. The general model of average acceleration is

$$\mathbf{a}\mathrm{d}t = \mathrm{d}\boldsymbol{v}. \tag{14}$$

Thus, integration w.r.t. time in interval $\Delta t = t_2 - t_1$, and highlighting that acceleration $\hat{\mathbf{a}}$ is the sensor measurement,

$$\int_{v_1}^{v_2} \mathrm{d}\boldsymbol{v} = \hat{\mathbf{a}} \int_{t_1}^{t_2} \mathrm{d}t. \tag{15}$$

Developing and algebraically arranging the previous equation for two dimensions yields the following:

$$\boldsymbol{v} = \begin{pmatrix} \dot{x}_t \\ \dot{y}_t \end{pmatrix} = \begin{pmatrix} \dot{x}_{t-1} \\ \dot{y}_{t-1} \end{pmatrix} + \begin{pmatrix} \hat{\dot{x}}_t \\ \hat{\dot{y}}_t \end{pmatrix} \Delta t. \tag{16}$$

Two components of acceleration $\hat{\mathbf{a}} = (\hat{\ddot{x}}, \hat{\ddot{y}})^\top$ are measured by the sensor and are used to calculate instantaneous acceleration $\hat{\mathbf{a}}$. As depicted by Fig. 6, two accelerometers a_1 and a_3 were fixed to the robot's body. a_i is the reference of a given inertial device. To find an exact solution for two dimensions, we require the use of at least two equations.

Proposition 5.1. *The trigonometric ratio is formulated by the accelerometers' measurement, the z-turn axis, and the Cartesian accelerometers' position by the next relationship:*

$$\frac{y_z - y^{a_j}}{x_z - x^{a_j}} = \int_t \left(\frac{\ddot{y}^{a_j}}{\ddot{x}^{a_j}} \right) \mathrm{d}t. \tag{17}$$

This proposition satisfies the stipulation that the jth accelerometer location (x^{a_j}, y^{a_y}) w.r.t. (x_z, y_z) has the same geometric ratio as the accelerometer readings $\int \ddot{y}^{a_j} / \ddot{x}^{a_j} \mathrm{d}t$, if and only if it is aligned with the robot's fixed frame. Thus, from this proposition the next theorem is presented, which states that an equation system can describe the behavioural z-turn axis location.

Theorem 5.2. *One linear equation describes a single accelerometer, and at least two speed measurements are required as a necessary and sufficient condition to infer* (x_z, y_z).

$$y_z - x_z \int_t \left(\frac{\ddot{y}_t^{a_1}}{\ddot{x}_t^{a_1}} \right) \mathrm{dt} = y^{a_1} - x^{a_1} \int_t \left(\frac{\ddot{y}_t^{a_1}}{\ddot{x}_t^{a_1}} \right) \mathrm{dt} \tag{18}$$

and

$$y_z - x_z \int_t \left(\frac{\ddot{y}_t^{a_3}}{\ddot{x}_t^{a_3}} \right) \mathrm{dt} = y^{a_3} - x^{a_3} \int_t \left(\frac{\ddot{y}_t^{a_3}}{\ddot{x}_t^{a_3}} \right) \mathrm{dt}. \tag{19}$$

This particular set of equations is algebraically rewritten and integrated w.r.t. time, according to Eq. (16). Thus, for device a_1,

$$y_z - \left(\frac{\dot{y}_{t-1}^{a_1} + \hat{\ddot{y}}_t^{a_1} \Delta t}{\dot{x}_{t-1}^{a_1} + \hat{\ddot{x}}_t^{a_1} \Delta t} \right) x_z = y^{a_1} - \left(\frac{\dot{y}_{t-1}^{a_1} + \hat{\ddot{y}}_t^{a_1} \Delta t}{\dot{x}_{t-1}^{a_1} + \hat{\ddot{x}}_t^{a_1} \Delta t} \right) x^{a_1}. \tag{20}$$

Likewise, the equation for device a_3 is

$$y_z - \left(\frac{\dot{y}_{t-1}^{a_3} + \hat{\ddot{y}}_t^{a_3} \Delta t}{\dot{x}_{t-1}^{a_3} + \hat{\ddot{x}}_t^{a_3} \Delta t} \right) x_z = y^{a_3} - \left(\frac{\dot{y}_{t-1}^{a_3} + \hat{\ddot{y}}_t^{a_3} \Delta t}{\dot{x}_{t-1}^{a_3} + \hat{\ddot{x}}_t^{a_3} \Delta t} \right) x^{a_3}. \tag{21}$$

Hereafter, by substituting some terms for the sake of easy when treating the system of equations algebraically, let us define $\zeta_i = (\dot{y}_{t-1}^{a_i} / \dot{x}_{t-1}^{a_i})$, $\eta_i = y^{a_i}$, and $\varrho_i = x^{a_i}$. The equation system is then arranged in matrix form, and solving for an analytical solution yields the following:

$$\begin{pmatrix} 1 & -\zeta_1 \\ 1 & -\zeta_3 \end{pmatrix} \cdot \begin{pmatrix} x_z \\ y_z \end{pmatrix} = \begin{pmatrix} \eta_1 - \varrho_1 \zeta_1 \\ \eta_3 - \varrho_3 \zeta_3 \end{pmatrix}. \tag{22}$$

Corollary 2. *Given a squared matrix, the Cramer theorem yields the z-turn model solution stated by*

$$x_z = \frac{-\zeta_3(\eta_1 - \varrho_1 \zeta_1) + \zeta_1(\eta_3 - \varrho_3 - \zeta_3)}{-\zeta_3 + \zeta_1} \tag{23}$$

and

$$y_z = \frac{\eta_3 - \varrho_3 \zeta_3 - \eta_1 + \varrho_1 \zeta_1}{-\zeta_3 + \zeta_1}. \tag{24}$$

In addition to Theorem 6.2 and Corollary 2, this idea is complemented by the kinematic effects yielded by the suspension angle behaviour γ_i through the factor l_i.

$$l_i = \sqrt{(\Delta x_i)^2 + (\Delta y_i)^2} \tag{25}$$

defined by the terms,

$$\Delta x_i = x_{w_i} - x_z \tag{26}$$

as well as the magnitude,

$$\Delta y_i = |y_{w_i} - y_z|. \tag{27}$$

The angles α_i denote the angular relationship between l_i w.r.t. the x-axis (counter-clockwise) as depicted by Fig. 5. Each α_i angle value varies according to l_i values, which are affected

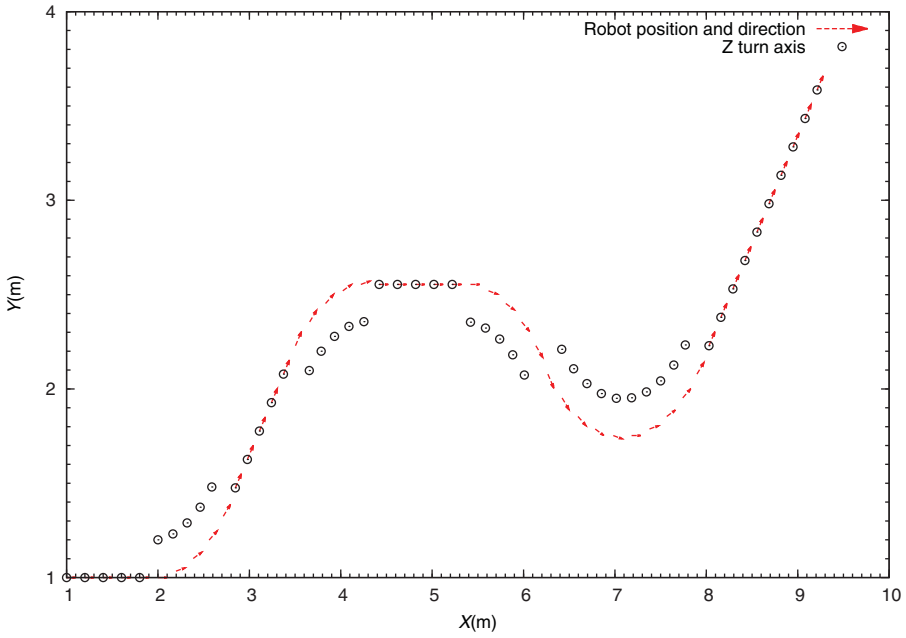

Fig. 7. Z-turn axis displacement (circles), with respect to the robot's pose (vectors).

by the suspension oscillations (Fig. 4). For $-y$, a negative arcsin sign is obtained with $\alpha_1 = 2\pi + \arcsin(\Delta y_1/l_1)$, and $\alpha_2 = \pi - \arcsin(\Delta y_2/l_2)$. For $-y$, a positive arcsin sign is obtained with $\alpha_3 = \arcsin(\Delta y_3/l_3)$, and $\alpha_4 = \pi - \arcsin(\Delta y_4/l_4)$. In addition, we may obtain a simplified expression for α by replacing the terms

$$\delta_i = \arcsin\left(\frac{\Delta y_i}{l_i}\right). \tag{28}$$

Hence,

$$\begin{aligned} \alpha_1 &= 2\pi + \delta_1 \\ \alpha_2 &= \pi - \delta_2 \\ \alpha_3 &= \delta_3 \\ \alpha_4 &= \pi - \delta_4. \end{aligned} \tag{29}$$

Likewise, the formulation of β_i to control the wheels' steering is

$$\begin{aligned} \beta_1 &= -\alpha_1 + \phi_1 \\ \beta_2 &= -\alpha_2 + \phi_2 \\ \beta_3 &= -\alpha_3 + \phi_3 \\ \beta_4 &= -\alpha_4 + \phi_4, \end{aligned} \tag{30}$$

where the variables ϕ_i are the direct angle measurement given by the encoders to quantify steering angles. For instance, when the wheels are set fixed (i.e., no steering), then $\phi_i = 0$. Without loss of generality, by applying Theorem 6.2 and Corollary 2, Fig. 7 depicts the robot's pose with its instantaneous z-turn axis relocated during a trajectory.

6. Motion Stability Analysis

When the inertial forces exceed the friction force between the four wheels contact points $\mathbf{p}_i = (x_i, y_i)^\top$ and the ground surface, the wheels may lose physical contact with the terrain surface. Thus, manoeuvrability efficiency and stability are disturbed. Although this paper's scope is limited to analysis of kinematics, for the purpose of explaining the conditions of stability, we need to introduce

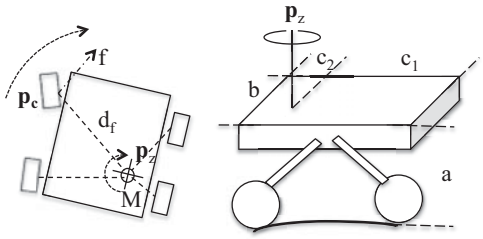

Fig. 8. Moment of inertia w.r.t. $\mathbf{p}_z$.

the dynamic formulation of the state equilibrium conditions. In Fig. 8 a depiction of the turning point $\mathbf{p}_z = (x_z, y_z)^\top$ is given (also represented by circles in Fig. 7), in which an instantaneous moment of inertia I_z is yielded. We consider only the strongest angular moment magnitude $M = I_z\alpha$ among the four wheels' contact points, because considering any other vehicle's mass point is meaningless. Separation of the wheels' contact point from the surface occurs due to exceeding magnitudes of z-axis moments of inertia I_z w.r.t. its farthest instantaneous wheel contact point, namely $\mathbf{p}_c$ and obtained by

$$d_f = \max_{1\le i\le 4} \|\mathbf{p}_z - \mathbf{p}_i\|.$$

Hence, the angle α_i that is maximized with d_f is given by α_f

$$\mathbf{p}_c = d_f \begin{pmatrix} \cos(\alpha_f) \\ \sin(\alpha_f) \end{pmatrix} \tag{31}$$

This is assumed to be the case when wheels strike no obstacles on the terrain surface that would forcibly separate the wheels from the ground. Nevertheless, our concerns is with the magnitudes of inertial effects that may yield instability. A vehicle's swift actions might continuously yield strong inertial moment effects. As a consequence, instability rises as $|\gamma_i|$ increases in magnitude. Thus, the case that better suits the situation was previously given in Proposition 4.3, for the angle γ_i as a function of $\dot{y}$ and $\ddot{y}$.

$$\gamma_i(\ddot{y}_s, \dot{y}_s) = \arcsin\left(\frac{m\mathrm{g} - m\ddot{y}_s - \kappa_v\dot{y}_s + \Delta_s}{\kappa_r d}\right).$$

Variations of I_z and $|\gamma_i(\dot{y}, \ddot{y})|$ contribute to separating the robot's centre of gravity from the ground, and damper effects occur more frequently, impacting the contact points' friction with the ground's surface. Thus, the wheels' vector point location $\mathbf{p}_i$ is given as,

$$\mathbf{p}_i = \left(\frac{d\cos(\gamma_i(\dot{y}, \ddot{y},))}{2}, \frac{b}{2}\right)^\top. \tag{32}$$

Hence, according to Fig. 8, the vehicles geometric parameters are defined as

$$c_{1,3} = \|\mathbf{p}_z - \mathbf{p}_{1,3}\|\cos(\alpha_{1,3}) \tag{33}$$

and

$$c_{2,4} = \|\mathbf{p}_z - \mathbf{p}_{2,4}\|\cos(\alpha_{2,4}). \tag{34}$$

Likewise, considering that the vehicle's height $\mathrm{a}(\gamma_i)$ changes over time in terms of γ_i,

$$\mathrm{a}(\gamma_i) = r + d\cos(\gamma_i) + \Delta_s \tag{35}$$

the robot's inertial moment is a mass property of a rigid non-uniform body, in which its inertial moment is located around its z-turn axis $\mathbf{p}_z$. Thus, the parallel theorem is applied for an arbitrary axis.

$$I = \int_{-c_2}^{c_1} \left(\frac{b^2}{12}\right) \frac{m}{c} \mathrm{dc}. \tag{36}$$

Then, after integrating the general expression,

$$I = \frac{m}{12}(b^2 + c^2). \tag{37}$$

Hence, substituting the variable limits, $c = c_1 + c_2$ (from Fig. 8), the z-turn axis inertial moment is given by

$$I = \frac{m}{12}\left(b^2 + (\|\mathbf{p}_z - \mathbf{p}_1\| \cos(\alpha_1) + \|\mathbf{p}_z - \mathbf{p}_2\| \cos(\alpha_2))^2\right). \tag{38}$$

Since the angular moment is equivalent to the torsional moment $M = I_z \mathrm{d}\omega/\mathrm{dt}$, we refer to the tangential effects on $\mathbf{p}_c$,

Proposition 6.1. *For the farthest wheel contact point $\mathbf{p}_c$ from the instantaneous spinning point $\mathbf{p}_z$, the tangential force f_T has the equivalence $I_z \mathrm{d}\omega/\mathrm{dt} \equiv f_T d_f$.*

$$I_z \frac{\mathrm{d}\omega_c}{\mathrm{dt}} = m \cdot a_T \|\mathbf{p}_z - \mathbf{p}_c\|. \tag{39}$$

The tangential acceleration a_T of the wheel point w.r.t. z-turn point $\|\mathbf{p}_z - \mathbf{p}_c\|$ is

$$a_T = \frac{I_z \dot{\omega}_c}{m\|\mathbf{p}_z - \mathbf{p}_c\|}. \tag{40}$$

Furthermore, a second proposition associated with the tangential force f_T is defined.

Proposition 6.2. *The instantaneous torsional moment M_z yielded w.r.t. $\mathbf{p}_z$ as a function of the kinetic and potential energies,*

$$M_z = f_T \|\mathbf{p}_z - \mathbf{p}_c\|. \tag{41}$$

The torsional moment expressed in terms of the Euler–Lagrange form,

$$M_z = \frac{\mathrm{d}}{\mathrm{dt}}\left(\frac{\partial \mathcal{L}}{\partial \dot{\mathbf{q}}}\right) - \frac{\partial \mathcal{L}}{\partial \mathbf{q}}, \tag{42}$$

where the generalized coordinate vector $\mathbf{q} = (v_c, \omega_c)^\top$ and $\dot{\mathbf{q}} = (\dot{v}_c, \dot{\omega}_c)^\top$ represent the kinematics of the actual wheel's contact point $\mathbf{p}_c$, where it exhibits more instantaneous inertial magnitude with tangential velocity v_c and angular velocity omega$_c$.

$$\mathcal{L} = \frac{1}{2} m v_c^2 + \frac{1}{2} I_z \omega_c^2$$

Therefore, the tangential force f_T of $\mathbf{p}_c$ is defined by

$$f_T = \frac{\|\frac{\mathrm{d}}{\mathrm{dt}}\left(\frac{\partial \mathcal{L}}{\partial \dot{\mathbf{q}}}\right) - \frac{\partial \mathcal{L}}{\partial \mathbf{q}}\|}{\|\mathbf{p}_z - \mathbf{p}_c\|}. \tag{43}$$

Thus, from Propositions 6.1 and 6.2, the inertial equilibrium conditions arises in Lemma 6.3,

Lemma 6.3. *The system has inertial stability when either of following equilibrium conditions occur:*

(a) If $a_c < \varepsilon_a$, $\mathbf{p}_c$ remains in contact with the ground's surface, where ε_a is the limit acceleration magnitude in terms of moment of inertia (Proposition 6.1).

$$\left| \frac{I_z \dot{\omega}}{m \|\mathbf{p}_z - \mathbf{p}_c\|} \right| < \varepsilon_a. \tag{44}$$

(b) If $f_T < \varepsilon_f$, $\mathbf{p}_c$ remains in contact with the ground's surface, where ε_f is the limit force magnitude in terms of energies (Proposition 6.2).

$$\frac{\|M_z\|}{\|\mathbf{p}_z - \mathbf{p}_c\|} < \varepsilon_f. \tag{45}$$

7. The Kinematic Control Law for Wheels

This section concerns the robot's kinematic analysis on the wheels' DOFs not yet discussed in $\dot{\varphi}_i$ and $\dot{\beta}_i$ and how they contribute to the robot's posture. Figure 5 depicts a description of the wheels steer angle $\beta_i \, \forall \, i = \{1, \ldots, 4\}$.

Lemma 7.1. *The robot's body motion $(\dot{x}_i, \dot{y}_i, \dot{\theta}_i)$ is partially contributed to by each ith with wheel tangential velocity $r\dot{\varphi}_i$ of nominal radius r and of angular speed $\dot{\varphi}_i$. A single-wheel contribution to the robot's motion is described by Eq.* (46)*,*

$$\begin{pmatrix} \dot{x}_i \\ \dot{y}_i \\ \dot{\theta}_i \end{pmatrix} = \frac{r}{4} \begin{pmatrix} \cos(\alpha_i + \beta_i) \\ \sin(\alpha_i + \beta_i) \\ \frac{\sin(\beta_i)}{l_i} \end{pmatrix} \varphi_i. \tag{46}$$

However, the translational and rotational velocities $\dot{\boldsymbol{\xi}} = (\dot{x}, \dot{y}, \dot{\theta})^\top$ of the whole robot are given as an average of all the wheels that are fixed to the system. The four-wheel restrictions along the centred wheel plane are described by expressions (47)–(49).

$$\dot{x} = \frac{r}{4} \sum_{i=1}^{4} \cos(\alpha_i + \beta_i) \dot{\varphi}_i \tag{47}$$

$$\dot{y} = \frac{r}{4} \sum_{i=1}^{4} \sin(\alpha_i + \beta_i) \dot{\varphi}_i. \tag{48}$$

In addition, see the model for $\dot{\theta}$ in terms of l_i, the latter discussed in previous section,

$$\dot{\theta} = \frac{r}{4} \sum_{i=1}^{4} \frac{\sin(\beta_i)}{l_i} \dot{\varphi}_i. \tag{49}$$

Thus, in stating the wheels' kinematic restrictions in vector form for a 4WD4S system, the wheels' plane restriction is governed by the vectors $\boldsymbol{\kappa}_i$. This is described by the following Eqs. (50)–(53).

$$\boldsymbol{\kappa}_1 = \left(\cos(\alpha_1 + \beta_1), \sin(\alpha_1 + \beta_1), \frac{\sin(\beta_1)}{l_1} \right)^\top \tag{50}$$

$$\boldsymbol{\kappa}_2 = \left(\cos(\alpha_2 + \beta_2), \sin(\alpha_2 + \beta_2), \frac{\sin(\beta_2)}{l_2}\right)^\top \tag{51}$$

$$\boldsymbol{\kappa}_3 = \left(\cos(\alpha_3 + \beta_3), \sin(\alpha_{3(t)} + \beta_3), \frac{\sin(\beta_3)}{l_3}\right)^\top \tag{52}$$

$$\boldsymbol{\kappa}_4 = \left(\cos(\alpha_4 + \beta_4), \sin(\alpha_4 + \beta_4), \frac{\sin(\beta_4)}{l_4}\right)^\top \tag{53}$$

such that the rolling conditions vectors of the four wheels comprise the transition non-squared matrix $\mathbf{K}$ containing all-wheel restrictions, given by

$$\mathbf{K} = (\boldsymbol{\kappa}_1 \quad \boldsymbol{\kappa}_2 \quad \boldsymbol{\kappa}_3 \quad \boldsymbol{\kappa}_4)\,. \tag{54}$$

Similarly, we define a vector of rotational velocities $\dot{\boldsymbol{\Phi}}$ to simplify the four-wheel system, and we include within it the constant term r.

$$\dot{\boldsymbol{\Phi}} = r\,(\dot{\varphi}_1 \quad \dot{\varphi}_2 \quad \dot{\varphi}_3 \quad \dot{\varphi}_4)^\top\,. \tag{55}$$

The functional form for each wheel speed $\dot{\varphi}_i$ is described by the third degree polynomial,

$$\dot{\varphi}_i(d_i) = a_0 + a_1 d_i + a_2 d_i^2 + a_3 d_i^3, \tag{56}$$

which is obtained from the response curve of the actuator device (i.e., a DC motor) with calibrated coefficient terms $a_0, \ldots, a_3$. The independent variable d_i is the ith digital variable at computer level to control the motor rotational speed[25] $\dot{\varphi}_i(d_i)$.

Thus, without loss of generality, we state the next corollary:

Corollary 3. *The control vector model for a 4W active system is described by the next Eq.* (57)*,*

$$\mathbf{u} = \frac{\mathbf{K} \cdot \dot{\boldsymbol{\Phi}}}{4}. \tag{57}$$

This equation describes the robot's local locomotion capabilities.

Furthermore, the $\mathbf{K}$ matrix is not a square and, except for the fixed suspensions and synchronous and differential steering modes, the inverse of the matrix does not have a trivial solution. For this reason the inverse of the matrix $\mathbf{K}_A^{-1}$ is obtained numerically. The inverse of the kinematic solution for the generalized system is given through a general inverse form of the non-squared transition matrix $\mathbf{K}$, namely a pseudo-inverse for linearly independent columns, where

$$\dot{\boldsymbol{\Phi}} = 4\mathbf{K}^\top \cdot (\mathbf{K} \cdot \mathbf{K}^\top)^{-1} \cdot \mathbf{u} \tag{58}$$

where the Moore–Penrose pseudo-inverse exists and is unique $\mathbf{K}^+ \cdot \mathbf{K} = \mathbf{I}$, such that $\mathbf{K}^+ = \mathbf{K}^\top \cdot (\mathbf{K} \cdot \mathbf{K}^\top)^{-1}$.

Moreover, the robot's forward kinematics solution is in principle given within a local inertial system. Nevertheless, its enhanced description of a global system may be described by Theorem 7.2.

Theorem 7.2. *The posture $\dot{\boldsymbol{\xi}}$ of a 4W system with active $\dot{\varphi}$, $\dot{\beta}$, and $\dot{\gamma}$ variables is controllable through the state Eq.* (59)*,*

$$\dot{\boldsymbol{\xi}}_{t+1} = \mathbf{R}(\theta) \cdot \dot{\boldsymbol{\xi}}_t + \mathbf{B}(\theta)\mathbf{u}_t + \mathbf{t}, \tag{59}$$

where $\mathbf{t} = (t_x, t_y, 0)^\top$ *is a translation vector, and* $\mathbf{R}$ *is the squared orthogonal Euler rotation matrix,* $\mathbf{R}(\theta)^\top = \mathbf{R}(\theta)^{-1}$.

$$\mathbf{R}(\theta) = \begin{pmatrix} \cos(\theta) & -\sin(\theta) & 0 \\ \sin(\theta) & \cos(\theta) & 0 \\ 0 & 0 & 1 \end{pmatrix}. \tag{60}$$

Hence, the squared transition matrix $\mathbf{B}$ *is defined by*

$$\mathbf{B}(\theta) = \begin{pmatrix} \cos(\theta) & 0 & 0 \\ \sin(\theta) & 0 & 0 \\ 0 & 0 & 1 \end{pmatrix}. \tag{61}$$

For instance, the recursive form to estimate the robot's position at time $t+1$ expanding the control vector $\mathbf{u}$, is stated. By assuming $\mathbf{t} = (0, 0, 0)^\top$, which means the common coordinate system origin is given at the robot's initial posture, we have

$$\dot{\boldsymbol{\xi}}_{t+1} = \mathbf{R} \cdot \dot{\boldsymbol{\xi}}_t + \frac{1}{4}\mathbf{B}(\theta) \cdot \mathbf{K}(\alpha, \beta) \cdot \dot{\boldsymbol{\Phi}}. \tag{62}$$

Thus, by algebraically expanding the expression (62), the general Eq. (63) for a four-wheel robot rises to allow multi-configuration of several four-drive/four-steer kinematic modalities:

$$\dot{\boldsymbol{\xi}}^I_{t+1} = \mathbf{R} \cdot \begin{pmatrix} \dot{x}_t \\ \dot{y}_t \\ \dot{\theta}_t \end{pmatrix} + \frac{r}{4}\mathbf{B}(\theta) \cdot \begin{pmatrix} \cos(\alpha_1+\beta_1) & \cos(\alpha_2+\beta_2) & \cos(\alpha_3+\beta_3) & \cos(\alpha_4+\beta_4) \\ \sin(\alpha_1+\beta_1) & \sin(\alpha_2+\beta_2) & \sin(\alpha_3+\beta_3) & \sin(\alpha_4+\beta_4) \\ \frac{\sin(\beta_1)}{l_1} & \frac{\sin(\beta_2)}{l_2} & \frac{\sin(\beta_3)}{l_3} & \frac{\sin(\beta_4)}{l_4} \end{pmatrix} \cdot \begin{pmatrix} \dot{\varphi}_1 \\ \dot{\varphi}_2 \\ \dot{\varphi}_3 \\ \dot{\varphi}_4 \end{pmatrix} \tag{63}$$

Finally, the next statement (4) is an inverse general solution, which results from the previous theorem.

Corollary 4. *The wheel velocity* $\Delta\dot{\varphi}$ *required to displace the robot from* $\boldsymbol{\xi}_t$ *to* $\boldsymbol{\xi}_{t+1}$ *in a global inertial system is modelled by* (64)*:*

$$\dot{\boldsymbol{\Phi}} = 4\mathbf{K}^\top \cdot (\mathbf{K} \cdot \mathbf{K}^\top)^{-1} \cdot \mathbf{B}^{-1} \cdot (\dot{\boldsymbol{\xi}}_{t+1} - \dot{\boldsymbol{\xi}}_t - \mathbf{t}). \tag{64}$$

This last Eq. (64) provides the wheel speed magnitudes required between the postures $\dot{\boldsymbol{\xi}}_{t+1}$ and $\dot{\boldsymbol{\xi}}_t$. However, the major contribution of this mathematical solution is that we now can manipulate the variables α_i, and β_i to associate their configuration with different four-drive/four-steer kinematic modalities, as will be discussed in next section.

8. Kinematic Multi-Configuration

In this section, we deduce the kinematic control-law transition matrix $\mathbf{K}$ for some structures to describe their locomotive modalities. To provide a better understanding, Fig. 1 depicts some related kinematic variables and parameters, and Fig. 9 illustrates three rovers with different kinematic configurations.

Configuration Fig. 10(a) has fixed suspensions and wheels. Lateral velocities are $v_1 = v_2 = v_r$, and $v_3 = v_4 = v_l$. For fixed suspensions, as well as the z-turn axis aligned in the robot's centre, the magnitudes of $\Delta x_i = \Delta x$, $\Delta y_i = \Delta y$, and the values of $l_i = l$ are set as constants.

The values are set as $\alpha_1 = 2\pi - \alpha$, $\alpha_2 = \pi + \alpha$, $\alpha_3 = \alpha$, and $\alpha_4 = \pi - \alpha$. In order to align the wheels' orientation with the robot's local reference x-axis, the value of the β angles are equal to the negative value of the respective α_n angles. With this assumption, it is not necessary to consider clockwise rotation of the left-side wheels. Thus, $\beta_1 = -\alpha_1$, $\beta_2 = -\alpha_2$, $\beta_3 = -\alpha_3$, and $\beta_4 = -\alpha_4$. By replacing the values β, α angles, the kinematic control matrix is obtained accordingly. Additionally,

Fig. 9. The evolution of research related to the Lab's rovers: (a) Fixed 4WD; (b) fixed 4WD with dampers; (c) 4WD/4WS with dampers.

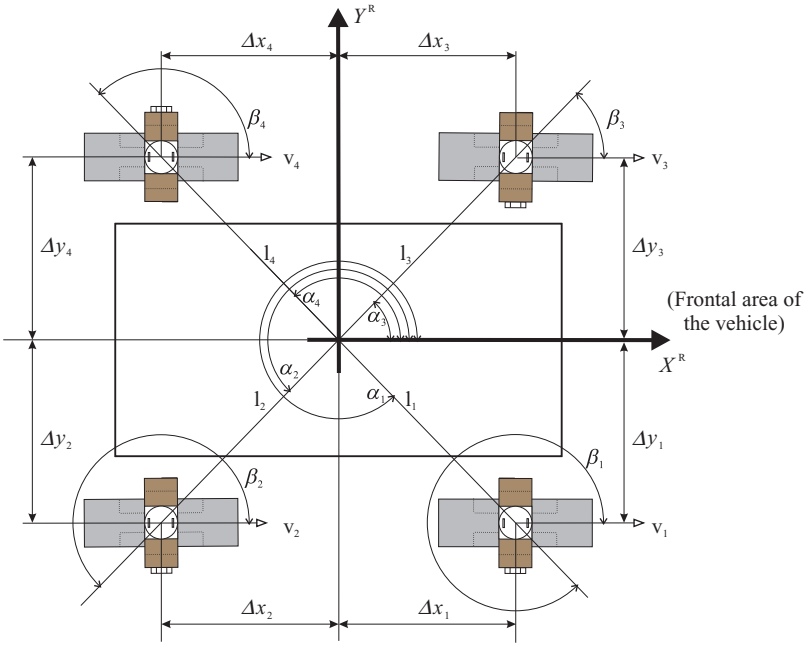

Fig. 10. Four-wheel configured as two-drives.

if we assign the value of $\alpha = \frac{\pi}{2}$, the resultant equation yields a kinematic model for a 2W differential-drive robot. This locomotion and steering configuration is depicted in Fig. 1(a) and is included in Table I in the non-holonomic group 1:NH. The values α_n, β_n angles, and l used for differential mode are restricted to fixed suspensions and steering angles. Thus, $\alpha_1 = 1/4\pi, \alpha_2 = 7/4\pi, \alpha_3 = 3/4\pi$, and $\alpha_4 = 5/4\pi$, and$\beta_i = -\alpha_i$. For this configuration mode, the vector of velocities for the right (wheels 1 and 2) and left (wheels 3 and 4) is described by the wheels' speed vector $\Phi = r(\dot{\varphi}_r, \dot{\varphi}_l)^\top$.

Through Eq. (54), a simplified restriction matrix (65) is obtained. The inverse matrix $\mathbf{K}$ obtained is described by (66).

$$\mathbf{K} = \begin{pmatrix} 2 & 2 \\ 0 & 0 \\ \frac{\sqrt{2}}{l} & -\frac{\sqrt{2}}{l} \end{pmatrix}. \tag{65}$$

It is likewise described by the inverse matrix solution given by

$$\mathbf{K}^{-1} = \frac{1}{4}\begin{pmatrix} 1 & 0 & l\sqrt{2} \\ 1 & 0 & -l\sqrt{2} \end{pmatrix}. \tag{66}$$

For simulation purposes, the wheel speeds ranged from 0 to 0.2m/s in alternate directions on both sides of the 4WD4S. The trajectory obtained in the global plane is depicted in Fig. 11.

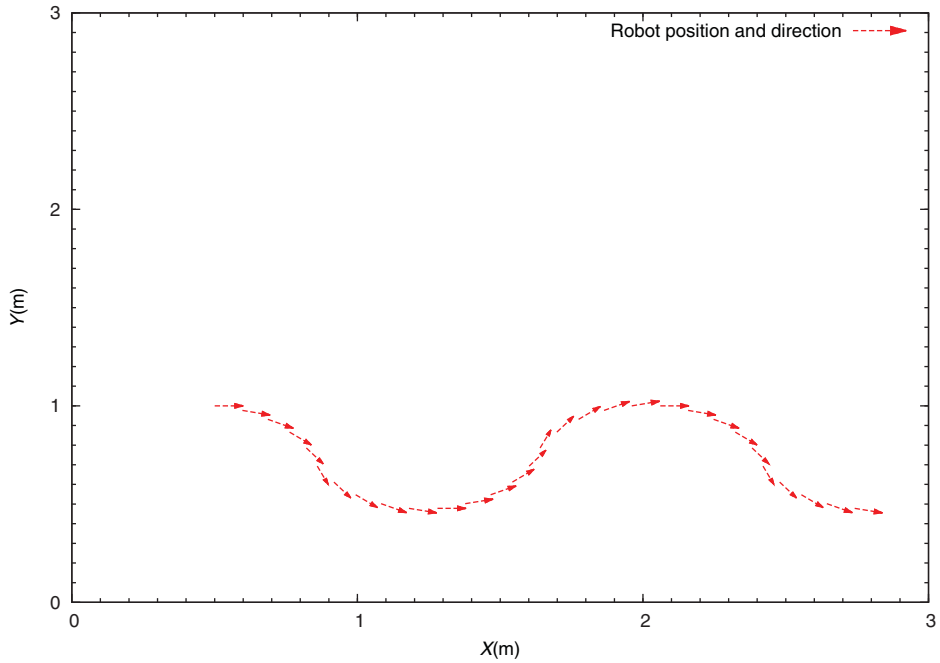

Fig. 11. Two-differential drive locomotion configuration trajectory.

Another numerical analysis case is depicted by Fig. 1(b), which concerns case 2 of Table I, 4W4D, and fixed wheels with no steering control. A simplified restriction vectors matrix (67) is algebraically obtained:

$$\mathbf{K} = \begin{pmatrix} 1 & 1 & 1 & 1 \\ 0 & 0 & 0 & 0 \\ \frac{1}{2}\frac{\sqrt{2}}{l} & \frac{1}{2}\frac{\sqrt{2}}{l} & -\frac{1}{2}\frac{\sqrt{2}}{l} & -\frac{1}{2}\frac{\sqrt{2}}{l} \end{pmatrix}. \tag{67}$$

Likewise, the inverse matrix $\mathbf{K}$ is described by (68). An issue with the differences between this configuration mode and the previous one already depicted by Fig. 1(a) is the difference in the velocity vectors of the wheels. For this case, all-wheel systems are explicitly described in $\dot{\mathbf{\Phi}} = r(\dot{\varphi}_1, \dot{\varphi}_2, \dot{\varphi}_3, \dot{\varphi}_4)^\top$.

$$\mathbf{K}^{-1} = \frac{1}{4}\begin{pmatrix} 1 & 0 & \sqrt{2}l \\ 1 & 0 & \sqrt{2}l \\ 1 & 0 & -\sqrt{2}l \\ 1 & 0 & -\sqrt{2}l \end{pmatrix}. \tag{68}$$

For the sake of simplicity in obtaining the matrix solution, we again considered a case with a fixed suspension, with no variations of α_i and β_i angles. The trajectory yielded over a Cartesian plane is depicted in Fig. 12.

One final arbitrary case within this manuscript's scope is an analysis of a drive/steer synchronous kinematic structure. The values for l_i, α_i, and β_i in each wheel are the same over time. The angle β_t was the only angle that showed synchronization of all wheels. Again for the sake of algebraic simplicity in the solution form, the suspension is considered fixed. Thus, α_i and l_i have the following constant values: $\alpha_1 = 1/4\pi$, $\alpha_2 = 7/4\pi$, $\alpha_3 = 3/4\pi$, $\alpha_4 = 5/4\pi$, and $\beta_i = -\alpha_i + \phi_i$. The transition matrix of the four-wheel kinematic restriction for an asynchronous robotic structure is given in a

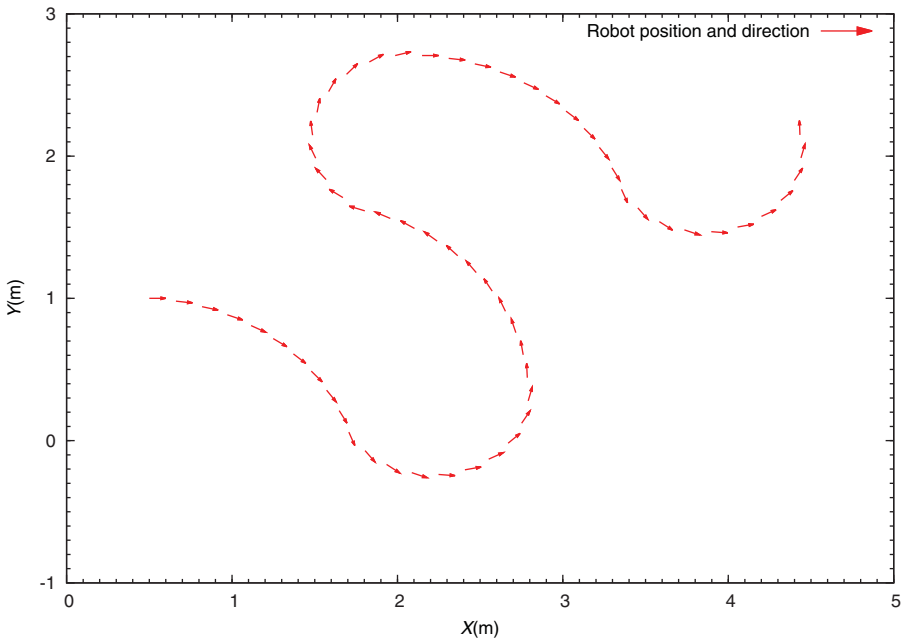

Fig. 12. 4W-differential drive (four asynchronous speeds) trajectory.

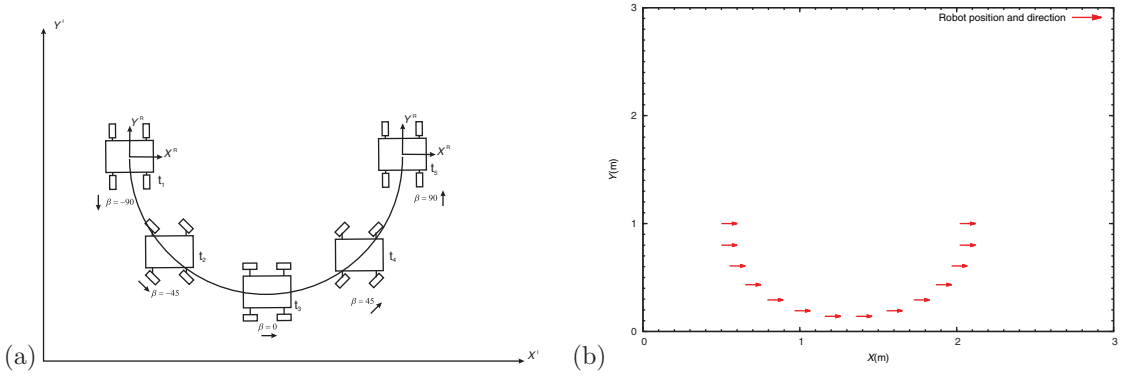

Fig. 13. (a) Robot's synchronous mode motion; *xy*-plane trajectory simulation (global plane).

simplified form by Eq. (69).

$$\mathbf{K} = \begin{pmatrix} \cos(\beta_t) & \cos(\beta_t) & \cos(\beta_t) & \cos(\beta_t) \\ \sin(\beta_t) & \sin(\beta_t) & \sin(\beta_t) & \sin(\beta_t) \\ \frac{\sin(\frac{\pi}{4}+\beta_t)}{l} & \frac{\cos(\frac{\pi}{4}+\beta_t)}{l} & -\frac{\cos(\frac{\pi}{4}+\beta_t)}{l} & -\frac{\sin(\frac{\pi}{4}+\beta_t)}{l} \end{pmatrix}. \tag{69}$$

Likewise, the inverse of the matrix $\mathbf{K}$ is described by (70).

$$\mathbf{K}^{-1} = \frac{1}{4} \begin{pmatrix} \cos(\beta_t) & \sin(\beta_t) & 2\sin(\frac{\pi}{4}+\beta_t)l \\ \cos(\beta_t) & \sin(\beta_t) & 2\cos(\frac{\pi}{4}+\beta_t)l \\ \cos(\beta_t) & \sin(\beta_t) & -2\cos(\frac{\pi}{4}+\beta_t)l \\ \cos(\beta_t) & \sin(\beta_t) & -2\sin(\frac{\pi}{4}+\beta_t)l \end{pmatrix} \tag{70}$$

Figure 13 shows a numerical simulation of the trajectory obtained by the synchronous drive/steer locomotion configuration. It starts at a steering angle of -90°, increments at $15^\circ/s$, and has

all-wheel speed of 0.2 m/s. The robot's initial location is $x_0 = 0.5$ m, $y_0 = 1.0$ m, $\theta_0 = 0$ degrees.

9. Conclusion

In this study, we found that an all-active kinematic multi-configuration model is suitable for a wide range of research studies. The general inverse/direct kinematic control law can be used for trajectory generation, path-following, trajectory control, as well as navigational algorithms with partial or full holonomy. From numerical experiments, we concluded that integrating a larger number of DOFs into a kinematic model, resulted in greater control of manoeuvrability and stability, regardless of the increased mathematical complexity. We also concluded that the inference of the mobile z-turn axis must be an essential aspect for the manoeuvrability of vehicles. Still, we believe that significant further research must be carried out to find new z-turn inference models. Effective z-turn axis calculations will improve the estimation of stability effects in damper-based wheeled platforms. Inferring the spinning vertical axis with respect to the wheels' longitudinal location resulted in a practical and low-cost solution. Also, the strategic combination of several accelerometer devices at arbitrary locations proved to be a powerful strategy, since for each accelerometer device on the robot's rigid body one linear equation is produced. Thus, we found that the more equations the system (or devices) have, the more accurate inference of the z-turn axis becomes. Both analytic and numerical models were proposed for robotic systems where all wheels are either steer, drive, or both steer and drive simultaneously. The proposed mechanical design was analysed for 12 DOFs, including wheel yaw, wheel rolling, and wheel-suspension pitch. The suspension pitch damper effects feature the robot because the wheel contact points are not fixed. In further exploration of stability issues, the moment of inertia and the angular moment were included in this work. We stated two general stability conditions in terms of the farthest wheel contact point from the z-turn instantaneous location. Such stability conditions constrain the situations when wheels may lose touch with the terrain's surface. Thus, we consider that the same accelerometers devices used to infer the z-turn axis, may in the future be combined with one gyroscope to measure inertial effects in terms of forces, accelerations, and Lagrangian magnitudes. Future works may include the functional forms of forces based on the results of this work, including numerical calculation of lateral and longitudinal turn axes to increase robustness of stability control. Also, force and pressure sensors will be explicitly used to control the active dampers.

References

1. J. C. Alexander and J. H. Maddocks, "On the kinematics of wheeled mobile robots," *I. J. Robotic Res.* **8**(5), 15–27 (1989).
2. S. Arslan and H. Temeltas, "Robust Motion Control of a Four Wheel Drive Skid-Steere Mobile Robot," *Proceedings of the 7th International Conference on Electrical and Electronics Engineering*, vol. 2 (2011) pp. 415–419.
3. J. Baillieul, "Avoiding Obstacles and Resolving Kinematic Redundancy," *Proceedings of the IEEE International Conference on Robotics and Automation*, vol. 3 (1986) pp. 1698–1704.
4. P. W. Bartlett, D. Wettergreen and W. Whittaker, "Design of the Scarab Rover for Mobility and Drilling in Lunar Cold Traps," *International Symposium on Artificial Intelligence, Robotics and Automation in Space,* (2008).
5. A. Bouloubasis and G. McKee, "The Mobility System of the Multi-Tasking Rover (mtr)," *IEEE International Conference on Robotics and Automation* (2007) pp. 4919–4924.
6. G. Campion, G. Bastin and B. d'Andréa Novel, "Structural properties and classification of kinematic and dynamic models of wheeled mobile robots," *IEEE Trans. Robot. Autom.* **12**(1), 47–62 (1996).
7. L. Cocco and S. Rapuano, "Accurate Speed Measurement Methodologies for Formula One Cars," *Proceedings of the Instrumentation and Measurement Technology Conference IMTC 2007. IEEE* (2007) pp. 1–6.
8. F. Cordes, A. Dettmann and F. Kirchner, "Locomotion Modes for a Hybrid Wheeled-Leg Planetary Rover," *IEEE International Conference on Robotics and Biomimetics (ROBIO)* (2011) pp. 2586–2592.
9. Song Yong-duan, Chen He-nan and Li Dan-yong "Virtual-point-based fault-tolerant lateral and longitudinal control of 4W-steering vehicles," *IEEE Trans. Intell. Transp. Syst.* **12**(4), 1343–1351 (Dec. 2011).
10. R. Solea, A. Filipescu, V. Minzu and S. Filipescu, "Sliding-Mode Trajectory-Tracking Control for a Four-Wheel-Steering Vehicle," *Proceedings of the 8th IEEE International Conference on Control and Automation* (Jun. 2010), IEEE, pp. 382–387.

11. G. Freitas, G. Gleizer, F. Lizarralde, L. Hsu and N. R. S. dos Reis, "Kinematic reconfigurability control for an environmental mobile robot operating in the amazon rain forest," *J. Field Robot.* **27**(2), 197–216 (Mar. 2010).
12. R. Grepl, J. Vejlupek, V. Lambersky, M. Jasansky, F. Vadlejch and P. Coupek, "Development of 4ws/4wd Experimental Vehicle: Platform for Research and Education in Mechatronics," *IEEE International Conference on Mechatronics (ICM)* (2011) pp. 893–898.
13. H. W. Home, "Can we utilize the rear wheels of FF cars?," Available at: http://world.honda.com/history/challenge/19874ws/ (Apr. 2013).
14. K. Iagnemma, A. Rzepniewski, S. Dubowsky, P. Pirjanian, T. Huntsberger, and P. Schenker, "Mobile robot kinematic reconfigurability for rough-terrain," **In** *Proceedings SPIE's International Symposium on Intelligent Systems and Advanced Manufacturing*, Aug. 2000.
15. K. Iagnemma, A. Rzepniewski, S. Dubowsky and P. Schenker, "Control of robotic vehicles with actively articulated suspensions in rough terrain," *Auton. Robots* **14**, 5–16 (2003).
16. M. R. Inc, "Pioneer, 3-at", Online Available at: http://www.mobilerobots.com/ResearchRobots/P3AT.aspx (Apr. 2013).
17. M. R. Inc, "Seekur, autonomous all-weather robot," Online Available at: http://www.mobilerobots.com/ResearchRobots/Seekur.aspx (Apr. 2013).
18. S. R. Inc, "Segway, announces its newest rmp – arti," Online Available at: http://rmp.segway.com/2012/10/09/segway-announces-its-newest-rmp-arti/ (Apr. 2013).
19. I. M. Johnston, "Worlds best tractor in 1910!" Online Available at: http://www.greenmountpress.com.au/cottongrower/Back%20issues/281fmcot07/54_TractorTales.pdf (Feb. 2007).
20. M. Kasahua and Y. Mori, "Trajectory tracking control of the four-wheel vehicle according to speed change," *SICE Annu. Conf.* **201**, 3449–3452 (2010).
21. T. Hiraoka, O. Nishihara and H. Kumamoto, "Automatic path-tracking controller of a four-wheel steering vehicle," *Vehcicle Syst. Dyn.* **47**(10), 1205–1227 (Oct. 2009).
22. A. A. Maciejewski and C. A. Klein, "Obstacle avoidance for kinematically redundant manipulators in dynamically varying environments," *Int. J. Robot. Res.* **4**, 109–117 (1985).
23. A. Mandow, J. Martinez, J. Morales, J.-L. Blanco, A. Garcia-Cerezo and J. Gonzalez, "Experimental Kinematics for Wheeled Skid-Steer Mobile Robots," *IEEE/RSJ International Conference on Intelligent Robots and Systems, IROS* (2007) pp. 1222–1227.
24. E. Martínez-García and R. Torres-Cordoba, "4wd Skid-Steer Trajectory Control of a Rover with Spring-Based Suspension Analysis," **In** *Intelligent Robotics and Applications* (H. Liu, H. Ding, Z. Xiong and X. Zhu, eds.) Lecture Notes in Computer Science, vol. 6424 (Springer, Berlin Heidelberg, 2010) pp. 453–464.
25. E. Martinez-Garcia and R. Torres-Cordoba, "Exponential fields formulation for wmr navigation," *J. Appl. Bionics Biomech.* **9**(4), 375–397 (2011).
26. A. Ollero-Baturone, *Robótica: Manipuladores y Robots Móviles* (Marcombo, Barcelona, España, 2001).
27. G. Reina, "Cross-coupled control for all-terrain rovers," *Sensors* **13**(1), 785–800 (2013).
28. B. Shamah, D. Apostolopoulos, E. Rollins and W. red Whittaker, "Field Validation of Nomads Robotic Locomotion," *Proceedings of the 1998 SPIE International Conference on Mobile Robots and Intelligent Transportation Systems* (1998) pp. 214–222.
29. B. Siciliano and O. Khatib, *Springer Handbook of Robotics* (Springer-Verlag New York, Inc., Secaucus, NJ, USA, 2007).
30. S. Tao Peng and J. Jia Sheu, "An Anti-Skidding Control Approach for Autonomous Path Tracking of a 4ws/4wd Vehicle," *Proceedings of the 7th Asian Control Conference* (2004) pp. 617–622.
31. M. Tarokh, H. D. Ho and A. Bouloubasis, "Systematic kinematics analysis and balance control of high mobility rovers over rough terrain," *Robot. Auton. Syst.* **61**(1), 13–24 (2013).
32. E. Grabianowski "How the Jeep Hurricane works," Online Available at: https://s3-ap-southeast-1.amazonaws.com/erbuc/files/5747_75d016c7-a01b-426a-95b3-dfedced2f6b2.pdf (Apr. 2013).
33. In Depth tutorials and information, "Four-wheel steering (4WS)", Online Available at: http://what-when-how.com/automobile/four-wheel-steering-4ws-automobile/ (Apr. 2013).
34. Nissan motor company, "4 wheel active steer (4WAS)," Online Available at: http://www.nissan-global.com/EN/DOCUMENT/PDF/TECHNOLOGY/TECHNICAL/4was_en.pdf (Apr. 2013).
35. D. Wettergreen, D. Jonak, D. Kohanbash, S. Moreland, S. Spiker and J. Teza, "Field experiments in mobility and navigation with a lunar rover prototype," **In**: *Field and Service Robotics* (A. Howard, K. Iagnemma and A. Kelly, eds.) Springer Tracts in Advanced Robotics, vol. 62 (Springer, Berlin Heidelberg, 2010) pp. 489–498.
36. H. Xu, D. Tan, Z. Zhang, K. Xue and B. Jin "A Reconfigurable Mobile Robot with 5th Wheel," *International Conference on Mechatronics and Automation, ICMA 2009* (2009) pp. 211–216.
37. H. Xu, Z. Zhang, Y. Wu and L. He, "Contact Angle Estimation Based on Kinematics Modeling Analyses for Rover with Caster and Camber," *IEEE International Conference on Robotics and Biomimetics (ROBIO)* (2010) pp. 137–142.
38. S. Y. J. O. K. Yi, "Coordinated control of hybrid 4wd vehicles for enhanced maneubrability and lateral stability," *IEEE Trans. Veh. Technol.* **61**(4), 1946–1950 (2012).